Title

Controlled Formation and Binding Selectivity of Discrete Oligo(methyl methacrylate) Stereocomplexes

Journal

Journal of the American Chemical Society, 140(5)

ISSN

0002-7863

Authors

Ren, Jing M
Lawrence, Jimmy
Knight, Abigail S
et al.

Publication Date

2018-02-07

DOI

10.1021/jacs.7b13095

Peer reviewed

HHS Public Access

Author manuscript

J Am Chem Soc. Author manuscript; available in PMC 2020 June 02.

Published in final edited form as:

J Am Chem Soc. 2018 February 07; 140(5): 1945–1951. doi:10.1021/jacs.7b13095.

Controlled Formation and Binding Selectivity of Discrete Oligo(methyl methacrylate) Stereocomplexes

Jing M. Ren[†,⊥], **Jimmy Lawrence**[†], **Abigail S. Knight**[†], **Allison Abdilla**[†], **Raghida Bou Zerdan**[†], **Adam E. Levi**[†], **Bernd Oschmann**[†], **Will R. Gutekunst**[†], **Sang-Ho Lee**[†], **Youli Li**[†], **Alaina J. McGrath**[†], **Christopher M. Bates**[‡,§], **Greg G. Qiao**[*,⊥], **Craig J. Hawker**[*,†,‡]

[†]Materials Research Laboratory, University of California, Santa Barbara, Santa Barbara, California 93106, United States

[‡]Department of Materials, University of California, Santa Barbara, Santa Barbara, California 93106, United States

[§]Department of Chemical Engineering, University of California, Santa Barbara, Santa Barbara, California 93106, United States

[⊥]Department of Chemical Engineering, The University of Melbourne, Parkville, Victoria 3010, Australia

Abstract

The triple-helix stereocomplex of poly(methyl methacrylate) (PMMA) is a unique example of a multistranded synthetic helix that has significant utility and promise in materials science and nanotechnology. To gain a fundamental understanding of the underlying assembly process, discrete stereoregular oligomer libraries were prepared by combining stereospecific polymerization techniques with automated flash chromatography purification. Stereocomplex assembly of these discrete building blocks enabled the identification of (1) the minimum degree of polymerization required for the stereocomplex formation and (2) the dependence of the helix crystallization mode on the length of assembling precursors. More significantly, our experiments resolved binding selectivity between helical strands with similar molecular weights. This presents new opportunities for the development of next-generation polymeric materials based on a triple-helix motif.

Graphical Abstract

[*]**Corresponding Authors**: gregghq@unimelb.edu.au, hawker@mrl.ucsb.edu.

Supporting Information

The Supporting Information is available free of charge on the ACS Publications website at DOI: 10.1021/jacs.7b13095.

Experimental procedures and additional characterization data for OMMA and stereocomplexes (PDF)

The authors declare no competing financial interest.

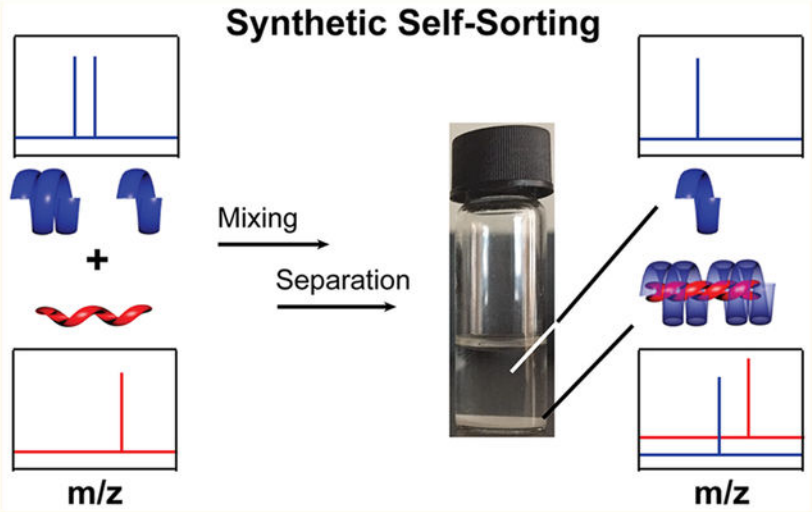

INTRODUCTION

From simple biological building blocks, nature assembles intricate structures with unrivaled properties and functions. Supramolecular biomolecule assemblies such as DNA[1] and collagen[2] are prime examples of the power of self-assembly to create complex nanostructures. In these cases, the assembly of linear chains into helical complexes serves as a powerful design motif for bioinspired materials broadly in the materials science and nanotechnology arenas.[3]

Synthetically, single-stranded helical structures based on poly(isocyanates), poly(triphenylmethyl methacrylates), and poly(acetylenes) are widely studied.[4–6] In contrast, multistranded synthetic helices have received significantly less attention with the triple-helix of stereoregular poly(methyl methacrylate), PMMA[7,8] being of prime importance. This supramolecular assembly consists of a double-stranded inner helix of *isotactic* (*it*-)PMMA, wrapped in a single-stranded outer helix of *syndiotactic* (*st*-)PMMA (Scheme 1). Interestingly, unlike natural multistranded helices, e.g., DNA, the *it*-/*st*- PMMA triple-helix does not require site-specific interactions such as $\pi-\pi$ stacking or hydrogen bonding to direct the helix formation. In this distinctive supramolecular system, van der Waals forces are responsible for driving the helical self-assembly of the PMMA chains.[9] Based on the unique structural features[7,10] of triple-helix PMMA stereocomplexes, a wide range of applications have been examined;[11–13] these include templates for inclusion complexes,[14,15] stereospecific polymerization,[16] and peptide recognition systems.[17,18]

Given this broad applicability, it is surprising that key parameters affecting the supramolecular assembly of PMMA stereocomplexes[19] remain unknown. Notable features such as the critical chain length[20] (defined as the degree of polymerization below which no stereocomplex formation occurs)[21,22] and the impact of molecular weight distribution (MWD)[23] on stereocomplex formation and crystallization remain unexplored. This lack of understanding has, in turn, limited the range of structures that can be prepared based on this triple-helix design motif. To address this challenge, well-defined stereoregular PMMA

derivatives were prepared by the combination of stereospecific polymerization and automated flash chromatography purification. Previously, small scale (up to tens of milligrams) separation of PMMAs has been performed via supercritical fluid chromatography (SFC) to isolate discrete PMMA species.[24] Using discrete *it*- and *st*-25mers isolated from repeated SFC separation, Ute et al.[24] prepared stereocomplex materials that showed a distinct melting transition, as opposed to a broad melting transition displayed by conventional stereocomplexes prepared from disperse materials. In comparison, our strategy allows scalable access[25] to libraries of stereoregular oligomers (Scheme 2).[26,27] Controlled self-assembly of these discrete or near-discrete building blocks[28–30] then permits the identification of critical parameters that drive stereocomplex formation,[24,27,31] leading to new insights and opportunities for synthetic helical assemblies with tunable properties.

RESULTS AND DISCUSSION

Discrete Stereoregular Oligomer Libraries.

The synthetic strategies for the preparation of highly stereoregular oligo(methyl methacrylate)s (OMMA)s are shown in Scheme 3.[32,33] As representative examples, multigram synthesis of *it*-OMMA (M_n = 1.2 kDa, $Đ$ = 1.2, mm/mr/rr = 80/10/10) was achieved through *tert*-butyl magnesium bromide (*t*BuMgBr)-mediated anionic polymerization of MMA (12 equiv). Similarly, initiation of the oligomerization of MMA (15 equiv) with 1,1-diphenyl-*n*-hexyllithium (*n*-Hex(Ph)$_2$Li) allowed the synthesis of *st*-OMMA (M_n = 1.9 kDa, $Đ$ = 1.2, mm/mr/rr = 1/24/75). By reducing initiator and monomer concentrations, side-reactions were minimized which allowed all oligomerizations and polymerizations to give well-defined stereoregular materials with controlled low MWs, narrow dispersities ($Đ_{GPC}$ < 1.3), and excellent yields (> 80%).

Multigram (up to 10 g) separation of the stereoregular OMMAs was achieved via automated silica-gel chromatography to give libraries of discrete and near-discrete stereoregular oligomers with a spectrum of different MWs (Figure 1, Table 1). A linear gradient elution profile of toluene and acetonitrile (0–50% v/v acetonitrile) was found to be successful for the isolation of both low and high DP oligomeric materials with remarkably low dispersities ($Đ_{MALDI}$ < 1.01). As an illustrative example (Figure 1), the separation of low dispersity *it*-OMMA ($M_{n,GPC}$ = 1.2 kDa, $Đ_{GPC}$ = 1.2) afforded discrete oligomers (DP = 5, 10, and 15) as confirmed by the ^{1}H NMR and MALDI-ToF MS analysis (Figure 1b, Table 1). The same separation strategy was subsequently applied to higher molecular weight *it*-OMMA ($M_{n,GPC}$ = 4.4 kDa, $Đ_{GPC}$ = 1.2) to give near-discrete oligomers with ultranarrow dispersities ($Đ$MALDI < 1.01) and DP values of up to 60 (Table 1). ^{1}H NMR, GPC, and MALDI-ToF MS characterization results confirmed the structural purity of all isolated *it*- and *st*-OMMAs with the dispersities of individual samples being significantly lower than that of the initial oligomer mixtures (Table 1, also see Supporting Information, SI 3).

Critical Chain Length Determination. To illustrate the importance of MW and dispersity control in the formation of OMMA-based triple-helices, preliminary evaluation of the critical chain length was attempted with traditional low dispersity materials (e.g., *it*-OMMA: DP_{NMR} = 11, $Đ_{GPC}$ = 1.2; *st*-OMMA: DP_{NMR} = 15, $Đ_{GPC}$ = 1.2; SI 4). However, the experimental results may lead to errors in the critical chain length identification, due to the

potential formation of minor amounts of stereocomplexes from high MW subspecies within the polydisperse precursors, highlighting the need for discrete oligomer materials. To address the critical chain length, a series of stereocomplex assemblies were therefore examined using the discrete oligomer libraries. In these cases, mixtures of *it*-/*st*-OMMA pairs (1:2 mass ratio) were prepared in acetonitrile/water (9:1),[34] dried, and analyzed via differential scanning calorimetry (DSC) and X-ray diffraction. From a range of samples, the critical length was found to be DP = 15 for *it*-OMMA and DP = 20 for *st*-OMMA (Figure 2).

When the chain length of both precursors was above these critical values, stereoregular OMMA pairs afforded aggregates of the semicrystalline triple-helices. For example, a 1:2 mixture of *it*-20 and *st*-20 exhibited an endothermic peak at 92 °C via DSC correlating to a semicrystalline material (Figure 3). In contrast, this melting peak is absent in the DSC traces of the individual *it*-and *st*-20 precursors and mixtures prepared from materials with chain lengths less than the critical value (e.g., *it*- 10 and *st*-20). In agreement with the DSC results, the X-ray diffraction (XRD) pattern of samples forming stereocomplexes(i.e., *it*-20/*st*-20 pair) show characteristic diffraction peaks of a typical PMMA triple-helix crystallite, with *d*-spacing values of2.0, 0.74, 0.60, and 0.57 nm, significantly different from the broad features in XRD traces of individual *it*-20 and *st*-20 OMMA samples.[35] This distinctive XRD pattern together with the DSC results also confirms the lower bound of chain length, with both *it*-15 and *st*-20 OMMAs being able to form a triple-helix stereocomplex.

According to the PMMA triple-helix stereocomplex model,[8] the critical chain lengths found in this work (15 and 20 repeat units for *it*- and *st*-OMMAs, respectively) are equivalent to 1.5 helical turns of the *it*-inner helix and a single helical turn of the *st*-outer helix. A possible explanation for the *it*-component requiring an extra 0.5 helical turn is that the lower molecular weight *it*-OMMA[34,36,37] precursors contain sequence defects at the chain ends (mm > 80%, SI 5) due to nonstereospecific initiation and termination.[38,39] This can impact the self-assembly and is in agreement with prior work demonstrated that a high level of stereoregularity of the *it*-component is required for stereocomplexation, compared to the *st*-counterpart.[34]Our assumption is further supported by the relative abundance of chains with perfect tacticity at critical chain length, which are 45% and 3% for *it*- and *st*-OMMA, respectively (SI 6). Although the *st*-component has a higher tolerance to defects, a longer critical chain length is still expected to compensate for the steric effects of the bulky diphenylhexyl chain end during stereocomplexation, and stabilize the resultant triple-helix.

Molecular Weight and Dispersity Effects.

After determining the critical length for each stereoregular OMMA, we investigated the effects of MW and dispersity of the OMMA precursors on stereocomplex formation. To illustrate the effect of dispersity, the stereocomplex formed from traditional low dispersity samples with an average DP of 20 (*it*-DP20: $M_{n,GPC}$ = 2.0 *k*Da, $Đ_{GPC}$ = 1.3; *st*-DP20: $M_{n,GPC}$ = 2.3 *k*Da, $Đ_{GPC}$ = 1.2) was compared with the corresponding stereocomplex prepared from near-discrete building blocks (*it*-20: $M_{n,MALDI}$ = 2.1 *k*Da, $Đ_{MALDI}$ = 1.003; *st*-20: $M_{n,MALDI}$ = 2.3 *k*Da, $Đ_{MALDI}$ = 1.005) (Figure 4). Though both the near-discrete and low dispersity OMMA mixtures were able to form OMMA stereocomplexes with the expected X-ray diffraction patterns (XRD, SI 7), the DSC curve of the disperse sample

shows a significantly wider melting transition (125–150 °C) than the curve for the discrete sample (Figure 4). These results suggest that an ensemble of triple-helix assemblies were formed from the low dispersity OMMAs, which aggregated into crystallites with a broad size distribution and different packing phases. In contrast, the stereocomplex assemblies formed from near-discrete building blocks led to uniform crystallites with a single sharp peak in the DSC trace.

This difference in thermal properties suggests tailoring of the melting temperatures for the stereocomplex can be achieved by varying the MW or dispersity of the oligomer building blocks. Such tunability gives access to a diverse range of semicrystalline materials with targeted melting temperatures. Using near-discrete OMMA building blocks, a series of helical “isomers” were prepared with the same overall helical length but different numbers of chains forming the outer helix. This was achieved by assembling a common isotactic, *it*-60 starting material with different *st*-OMMAs having DP of 20, 30, 40, and 60 (Figure 5, Complexes A–D). Remarkably, we found the melting temperature of the overall stereocomplexes increased with increasing DP of the *st*-components with melting transitions ranging from ≈100 °C to over 160 °C. It should also be noted that variable temperature XRD verified the disassembly of triple-helices over the melting temperature range (Figure SI 11a,b).

For higher MW oligomer stereocomplexes, two melting peaks were observed, which originate from melting of crystallites with different packing structures (Figure 5b–d). To gain more insight into the relationship between crystallization and molecular weight, a series of stereocomplexes were prepared from different molecular weight near-discrete OMMA starting materials. Interestingly, two different regimes were observed: At lower combined DP values, only a single melting temperature was observed, whereas two melting transitions were consistently observed for stereocomplex samples with combined DP values ≥ 90 (Figure 6). To explain these observations, we propose that the fringed-micellar crystallization mode prevails at low DP due to a faster rate of OMMA helix formation than crystallization (Figure SI 12a). This leads to the formation of crystallites that are more uniform in size and morphology. For the higher DP mixtures, we postulate that dual crystallization mechanisms are occurring, i.e., “fringed-micellar” and “lamellar” growth (Figure SI 12b) leading to different morphologies and crystallite sizes.[40,41]

To illustrate the potential of MW and MWD tailoring of stereocomplex properties, oligomer mixtures with customized MWDs were prepared by blending *it*-OMMA derivatives of different DP values with the same starting *st*-OMMA building block (*st*-40, SI 14). For example, a 1:1 combination of *it*-20 and *it*-60 with *st*-40 and a 1:1:1 combination of *it*-20, *it*-40, and *it*-60 with *st*-40 qualitatively gives the same average MW as a simple mixture of *it*-40 and *st*-40. Significantly, assembly of these “DP40” materials leads to stereocomplexes with markedly different melting profiles. The samples prepared from bimodal and trimodal *it*-40 samples were observed to have two melting peaks and a broad melting transition by DSC, whereas a single sharp melting peak was observed for the mixture formed from the single near-discrete *it*-OMMA starting material. We attribute these differences in melting properties to different triple-helix populations arising from changing molecular weight

distributions for the starting linear chains. As demonstrated above, the access to discrete and near-discrete oligomers allows control over the assembly and crystal growth processes.

Binding Selectivity.

For double-stranded DNA helices, helix stability is dictated by both complementary base pairing as well as the matching of individual strand lengths. For example, a DNA helix formed from two complementary strands is more stable than the same complex assembled from a long strand and two shorter complementary strands.[42] This phenomenon highlights the importance of strand lengths in stabilizing multistranded helical complexes. From the helical "isomer" experiments described above (Figure 5), we observed similar behavior for OMMA. Stereocomplexes with fewer helical components result in higher melting temperatures and increased stability as compared to the corresponding stereocomplexes containing a larger number of components. This difference can be significant for OMMA triple helices with a four-component assembly (Complex D) having a melting temperature 50–60 °C higher than the corresponding complex composed of eight components (Complex A).

In a further analogy with DNA and the ability of DNA complexes to undergo self-sorting to yield a more thermodynamically stable structure,[43] we hypothesized that a self-sorting phenomenon could be observed for a mixture of OMMA chains of different lengths. As detailed above, OMMA assembly favors the formation of a more stable triple-helix from the fewest total number of components. The selectivity could also be impacted by minimizing the number of chain ends and differences in solubility. This potential for molecular selectivity suggests that a mixture of OMMA chains could be sorted through stereocomplexation. To test this hypothesis, *it*-80 chains were mixed with an excess (2 equiv) of a 50:50 wt % mixture of *st*-25 and *st*-40 OMMA chains, and the precipitated stereocomplex was isolated from the supernatant that contained excess *st*-chains (Figure 7). Dissolution of the precipitate leads to individual chains that can then be analyzed and compared to the distribution of chains present in the supernatant. Discrete and near-discrete starting materials are enabling in this sorting experiment as the distribution of chains can be easily followed by GPC. From the 50:50 wt % mixture of an excess (2 equiv) of *st*-25 and *st*-40 OMMA chains with *it*-80 chains, two exclusively sorted stereocomplexes are possible, i.e., *st*-25/*it*-80, and *st*-40/*it*-80. Remarkably, on isolation of the precipitated stereocomplex and analysis by GPC, a 1:2 ratio of *st*-40 and *it*-80 chains was observed. In direct contrast, the supernatant consisted almost exclusively of uncomplexed *st*-25 chains, clearly indicating a self-sorting process (GPC Figure 7c,d and MALDI-ToF MS SI 15). The efficiency and robustness of self-sorting were then confirmed by the "sorting" of additional OMMA pairs containing different molecular weight *it*- and *st*-components (SI 16 and SI 17). It should be noted that a previous AFM study[9] revealed the preferential pairing of the same MW *it*-OMMA during stereocomplex formation. However, these self-sorting experiments illustrate the potential of binding selectivity in the design and formation of synthetic helical complexes.

CONCLUSION

We have investigated a series of OMMA stereocomplexes prepared from libraries of discrete and near-discrete stereoregular OMMAs ($Đ$ = 1.00–1.01). Enabled by this unique set of materials, key parameters that affect PMMA stereocomplex formation were evaluated. Additionally, synthetic guidelines were established that allow for the preparation of stereocomplexes with tailored melting properties and the development of self-sorting/separation protocols for OMMA derivatives. Inspired by the power of DNA-based nanotechnology,[43] this novel specificity may offer complementary functionality for assembling nanomaterials with increased synthetic and functional versatility.

Supplementary Material

Refer to Web version on PubMed Central for supplementary material.

ACKNOWLEDGMENTS

The research reported here was supported by the NSF MRSEC Program through DMR 1720256. These studies made use of shared facilities of the UCSB MRSEC (NSF DMR 1720256), a member of the Materials Research Facilities Network (www.mrfn.org). Additional support was provided by the Institute for Collaborative Biotechnologies through grant W911NF-09-0001 from the U.S. Army Research Office. The content of the information does not necessarily reflect the position or the policy of the government, and no official endorsement should be inferred. J.M.R. thanks the Victorian Endowment for Science, Knowledge and Innovation (VESKI) for a postdoctoral fellowship. A.S.K. was supported by a postdoctoral fellowship from the Arnold and Mabel Beckman Foundation. B.O. acknowledges the Alexander von Humboldt-Foundation for a Feodor Lynen Research Fellowship. W.R.G. thanks the NIH for a postdoctoral fellowship (F32GM108323).

REFERENCES

(1). Watson JD; Crick FHC Nature 1953, 171, 964–967. [PubMed: 13063483]

(2). Pauling L; Corey RB; Branson HR Proc. Natl. Acad. Sci. U.S. A 1951, 37, 205–211. [PubMed: 14816373]

(3). Yashima E; Ousaka N; Taura D; Shimomura K; Ikai T; Maeda K Chem. Rev 2016, 116, 13752–13990. [PubMed: 27754649]

(4). Cornelissen JJLM; Rowan AE; Nolte RJM; Sommerdijk NAJM Chem. Rev 2001, 101, 4039–4070. [PubMed: 11740926]

(5). Yashima E; Maeda K; Furusho Y Acc. Chem. Res 2008, 41, 1166–1180. [PubMed: 18690750]

(6). Nakano T; Okamoto Y Chem. Rev 2001, 101, 4013–4038. [PubMed: 11740925]

(7). Kumaki J; Kawauchi T; Okoshi K; Kusanagi H; Yashima E Angew. Chem., Int. Ed 2007, 46, 5348–5351.

(8). Christofferson AJ; Yiapanis G; Ren JM; Qiao GG; Satoh K; Kamigaito M; Yarovsky I Chem. Sci 2015, 6, 1370–1378. [PubMed: 29560224]

(9). Kumaki J; Kawauchi T; Ute K; Kitayama T; Yashima EJ Am. Chem. Soc 2008, 130, 6373–6380.

(10). Kumaki J; Kawauchi T; Yashima EJ Am. Chem. Soc 2005, 127, 5788–5789.

(11). Serizawa T; Hamada K.-i.; Kitayama T; Fujimoto N; Hatada K; Akashi M J. Am. Chem. Soc 2000, 122, 1891–1899.

(12). Kawauchi T; Kitaura A; Kumaki J; Kusanagi H; Yashima EJ Am. Chem. Soc 2008, 130, 11889–11891.

(13). Crne M; Park JO; Srinivasarao M Macromolecules 2009, 42, 4353–4355.

(14). Vidal F; Falivene L; Caporaso L; Cavallo L; Chen EYX J. Am. Chem. Soc 2016, 138, 9533–9547. [PubMed: 27388024]

(15). Kawauchi T; Kumaki J; Kitaura A; Okoshi K; Kusanagi H; Kobayashi K; Sugai T; Shinohara H; Yashima E Angew. Chem., Int. Ed 2008, 47, 515–519.

(16). Serizawa T; Hamada K.-i.; Akashi M Nature 2004, 429, 52–55. [PubMed: 15129276]

(17). Serizawa T; Sawada T; Kitayama T Angew. Chem., Int. Ed 2007, 46, 723–726.

(18). Serizawa T; Sawada T; Matsuno H; Matsubara T; Sato TJ Am. Chem. Soc 2005, 127, 13780–13781.

(19). Fox TG; Garrett BS; Goode WE; Gratch S; Kincaid JF; Spell A; Stroupe JD J. Am. Chem. Soc 1958, 80, 1768–1769.

(20). Schomaker E; Challa G Macromolecules 1986, 19, 2841–2846.

(21). Helary G; Belorgey G; Hogen-Esch TE Polymer 1992, 33, 1953–1958.

(22). Spěváček J; Schneider B Makromol. Chem 1974, 175, 2939–2956.

(23). Gentekos DT; Dupuis LN; Fors BP J. Am. Chem. Soc 2016, 138, 1848–1851. [PubMed: 26824147]

(24). Ute K; Miyatake N; Asada T; Hatada K Polym. Bull 1992, 28, 561–568.

(25). Lawrence J; Lee S-H; Abdilla A; Nothling MD; Ren JM; Knight AS; Fleischmann C; Li Y; Abrams AS; Schmidt BVKJ; Hawker MC; Connal LA; McGrath AJ; Clark PG; Gutekunst WR; Hawker CJ J. Am. Chem. Soc 2016, 138, 6306–6310. [PubMed: 27152711]

(26). Hatada K; Kitayama T; Ute K; Nishiura TJ Polym. Sci., Part A: Polym. Chem 2004, 42, 416–431.

(27). Ute K; Miyatake N; Osugi Y; Hatada K Polym. J 1993, 25, 1153–1160.

(28). van Genabeek B; de Waal BFM; Ligt B; Palmans ARA; Meijer EW ACS Macro Lett 2017, 6, 674–678. [PubMed: 28781926]

(29). Lawrence J; Goto E; Ren JM; McDearmon B; Kim DS; Ochiai Y; Clark PG; Laitar D; Higashihara T; Hawker CJ J. Am. Chem. Soc 2017, 139, 13735–13739. [PubMed: 28872865]

(30). Oschmann B; Lawrence J; Schulze MW; Ren JM; Anastasaki A; Luo Y; Nothling MD; Pester CW; Delaney KT; Connal LA; McGrath AJ; Clark PG; Bates CM; Hawker CJ ACS Macro Lett 2017, 6, 668–673.

(31). Nishiura T; Abe Y; Kitayama T Polym. J 2010, 42, 868–874.

(32). Hatada K; Ute K; Tanaka K; Kitayama T; Okamoto Y Polym. J 1985, 17, 977–980.

(33). Cao Z-K; Okamoto Y; Hatada K Kobunshi Ronbunshu 1986, 43, 857–861.

(34). Goh TK; Tan JF; Guntari SN; Satoh K; Blencowe A; Kamigaito M; Qiao GG Angew. Chem., Int. Ed 2009, 48, 8707–8711.

(35). Kawauchi T; Kumaki J; Okoshi K; Yashima E Macromolecules 2005, 38, 9155–9160.

(36). Ren JM; Satoh K; Goh TK; Blencowe A; Nagai K; Ishitake K; Christofferson AJ; Yiapanis G; Yarovsky I; Kamigaito M; Qiao GG Angew. Chem., Int. Ed 2014, 53, 459–464.

(37). Ren JM; Ishitake K; Satoh K; Blencowe A; Fu Q; Wong EHH; Kamigaito M; Qiao GG Macromolecules 2016, 49, 788–795.

(38). Hatada K; Ute K; Tanaka K; Imanari M; Fujii N Polym. J 1987, 19, 425–436.

(39). Ute K; Asada T; Miyatake N; Hatada K Makromol. Chem., Macromol. Symp 1993, 67, 147–155.

(40). Schomaker E; Challa G Macromolecules 1988, 21, 2195–2203.

(41). Schomaker E; Hoppen H; Challa G Macromolecules 1988, 21, 2203–2209.

(42). Protozanova E; Yakovchuk P; Frank-Kamenetskii MD J. Mol. Biol 2004, 342, 775–785. [PubMed: 15342236]

(43). Zhang DY; Seelig G Nat. Chem 2011, 3, 103–113. [PubMed: 21258382]

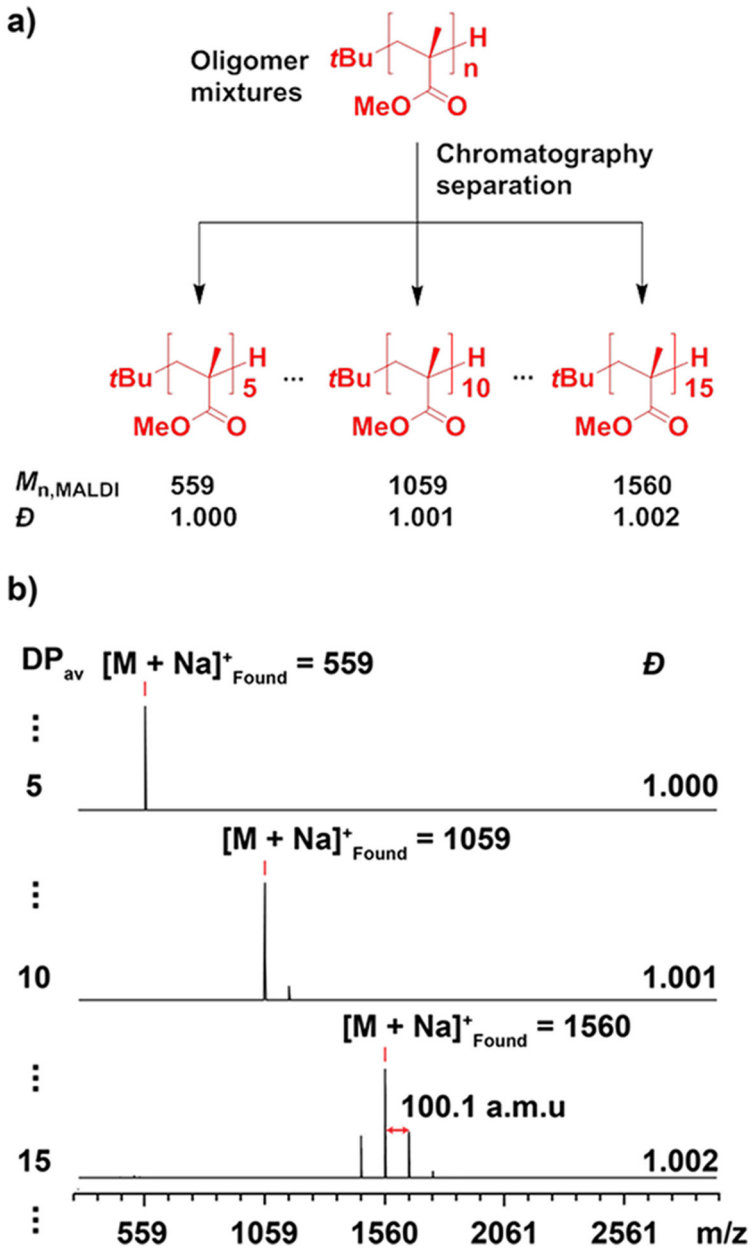

Figure 1.

(a) Schematic illustration of OMMA separation using low MW *it*-OMMA as an example. (b) MALDI-ToF mass spectra of the isolated *it*-OMMA samples (DP = 5, 10, and 15).

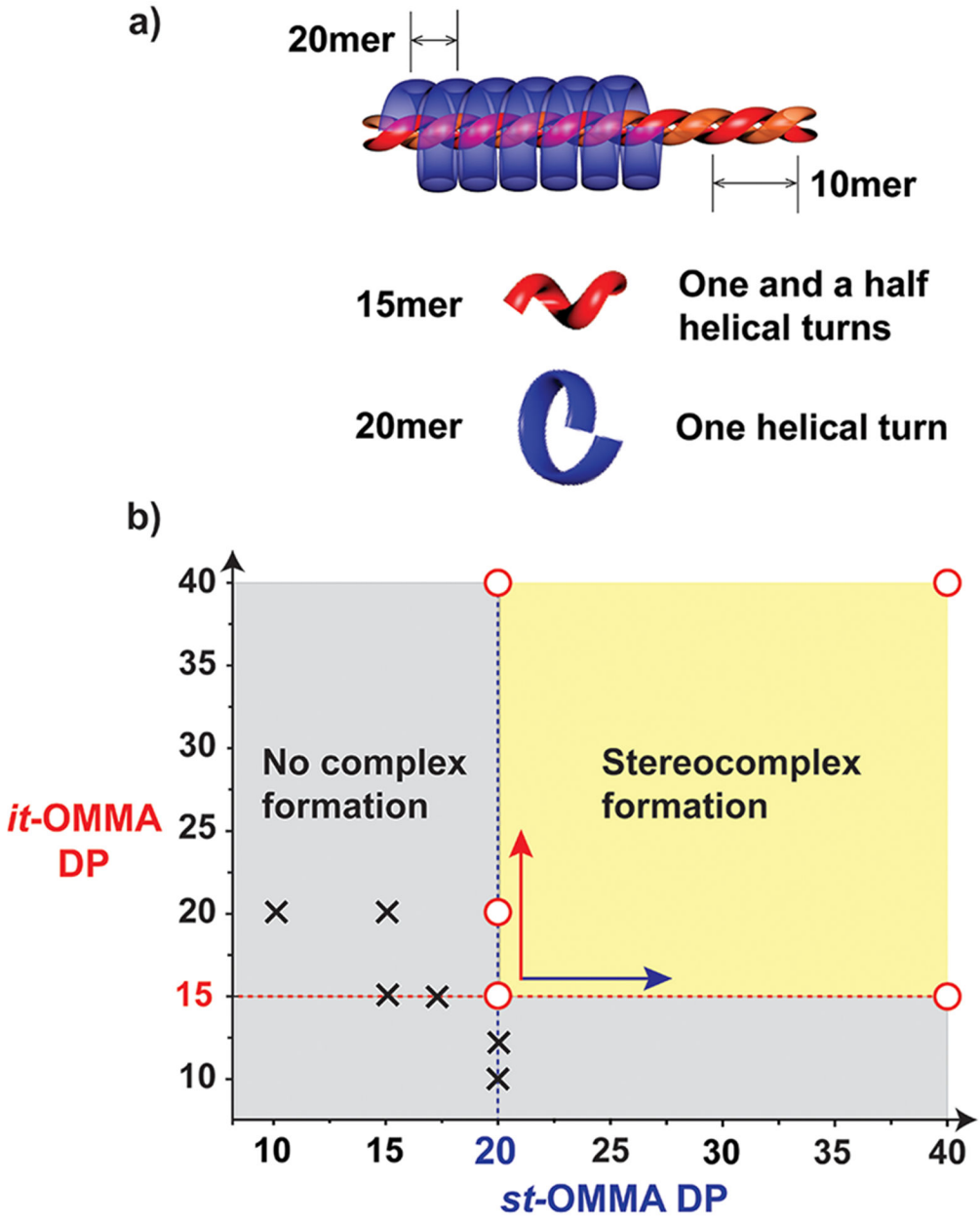

Figure 2.

(a) Schematic illustration of the minimal configurations of stereoregular OMMA helices. (b) Diagram illustrating the chain length requirements for *it*-/*st*-OMMAs to form the triple-helix stereocomplex, as determined by XRD and DSC. Circle (○) and cross (×) indicate complexation and no complexation observed, respectively.

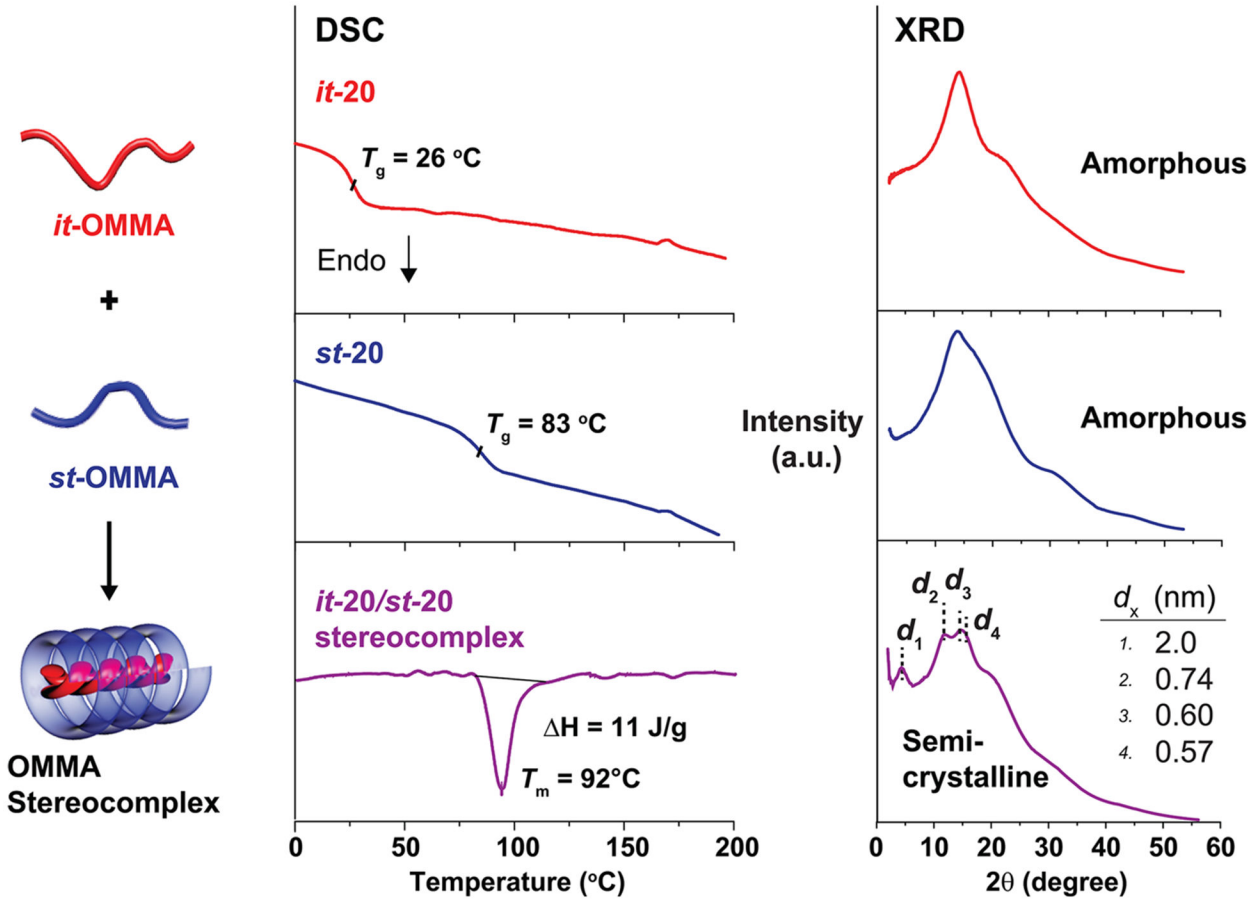

Figure 3.
DSC thermograms and XRD patterns of *it*-20, *st*-20, and their stereocomplex (*it*-/*st*- molar ratio = 1:2).

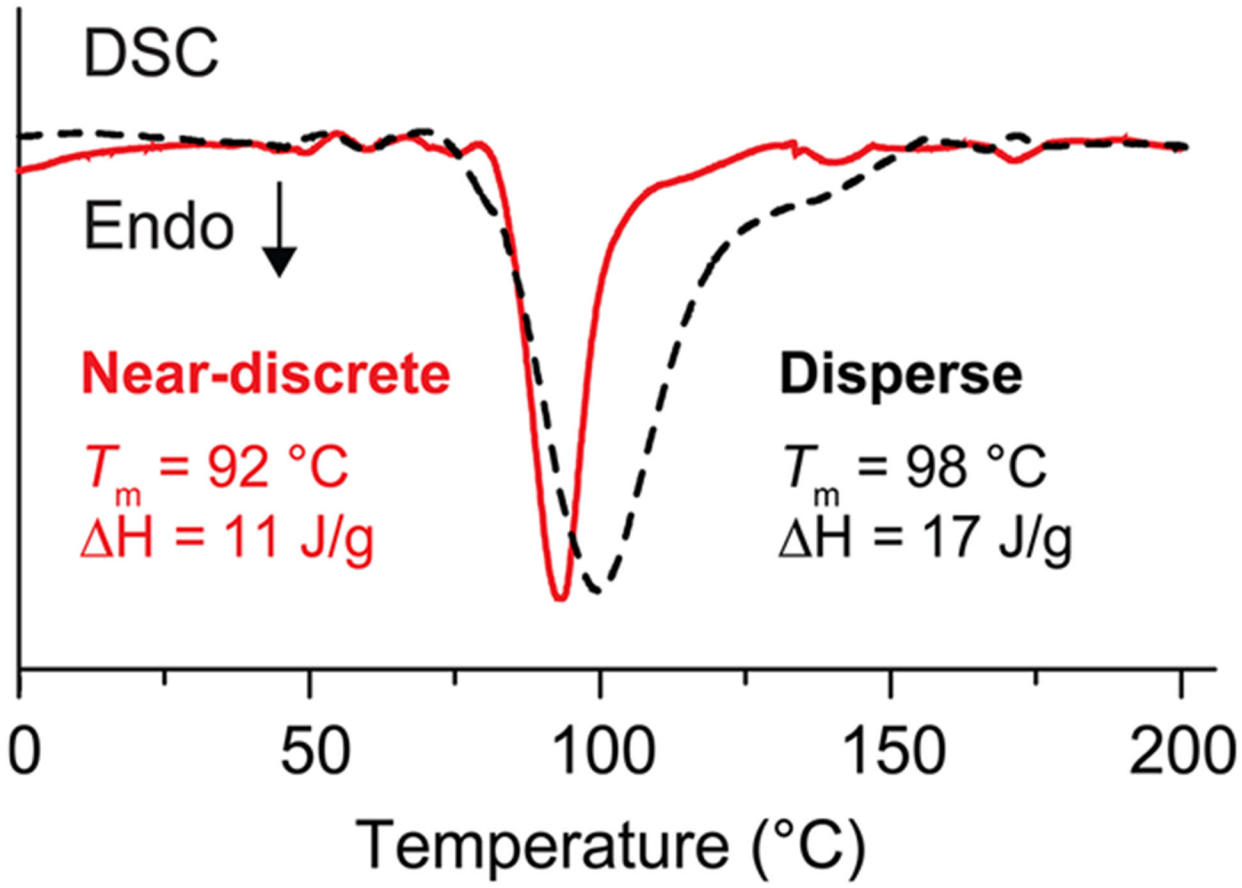

Figure 4.
DSC traces of the stereocomplexes prepared from near-discrete and disperse *it*-/*st*-oligomer pairs (DP_{av} = 20) (*it*-/*st*- molar ratio = 1:2).

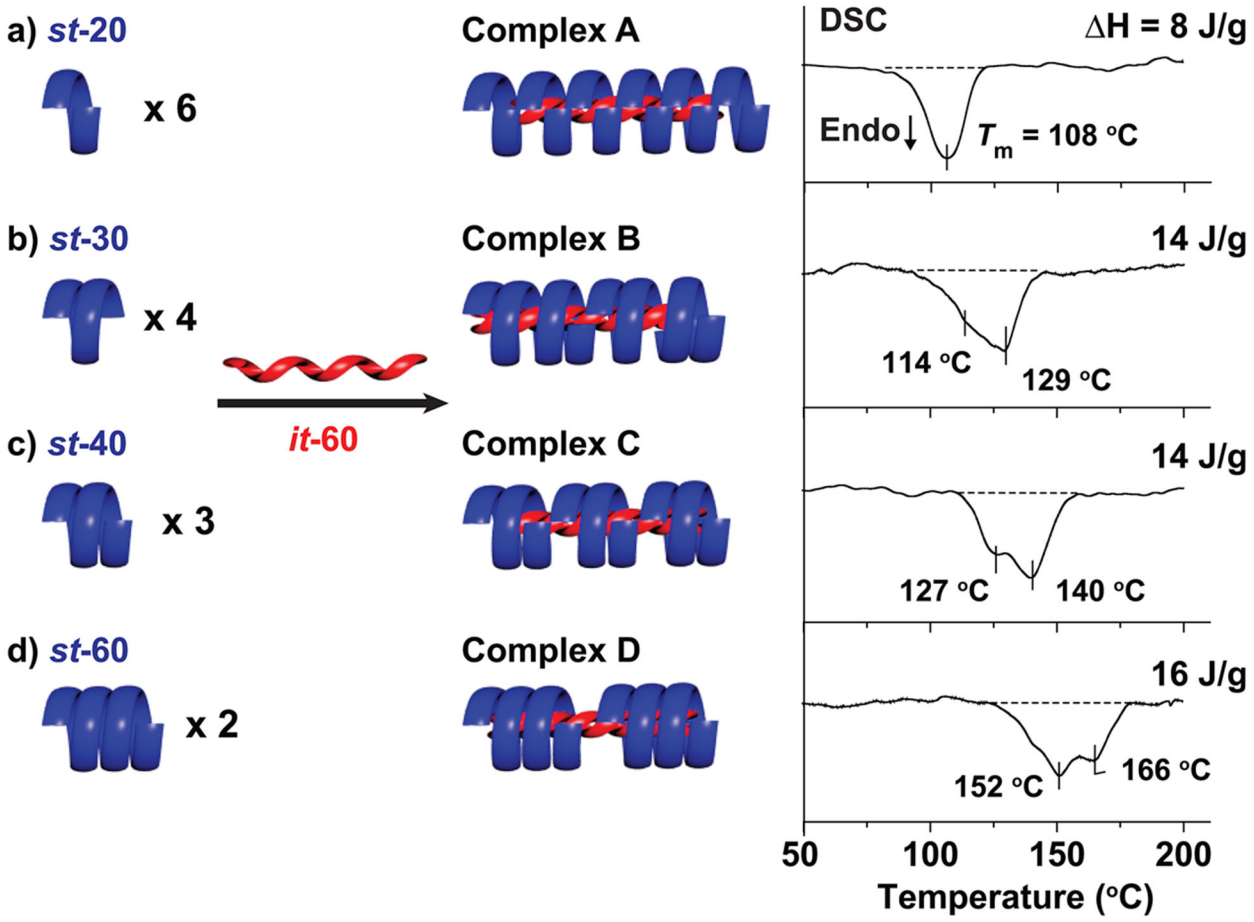

Figure 5.

Schematic illustration of a series of helical "isomers" with the same total helical length, prepared from *it*-60 with (a) *st*-20, (b) *st*-30, (c) *st*-40, and (d) *st*-60 samples, respectively (*it*-/*st*- molar ratio = 1:2).

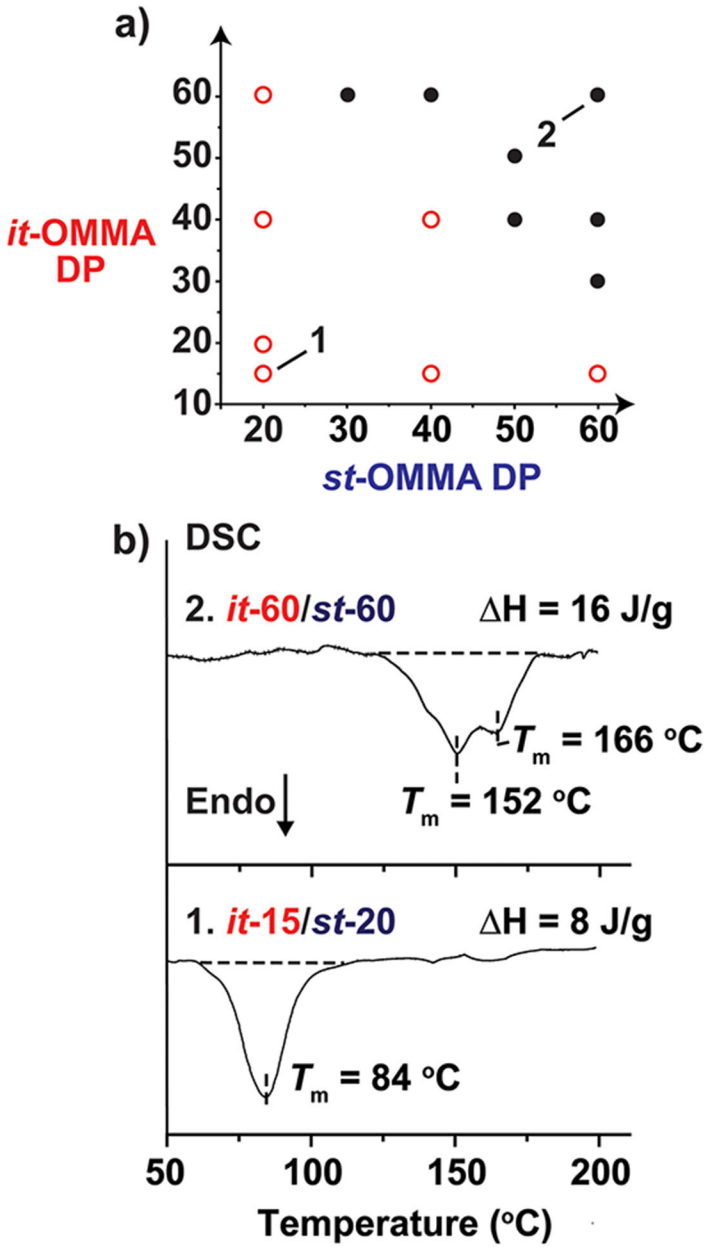

Figure 6.

(a) Diagram illustrating the melting behavior of OMMA stereocomplexes as a function of *it*-/*st*-OMMA chain lengths. Open (○) and closed (●) circles refer to samples with one and two melting peaks, respectively. (b) Differential scanning calorimetry (DSC) profiles of two illustrative stereocomplex examples (i.e., *it*-60/*st*-60 and *it*-15/*st*-20) showing melting transitions with two peaks and a single peak, respectively.

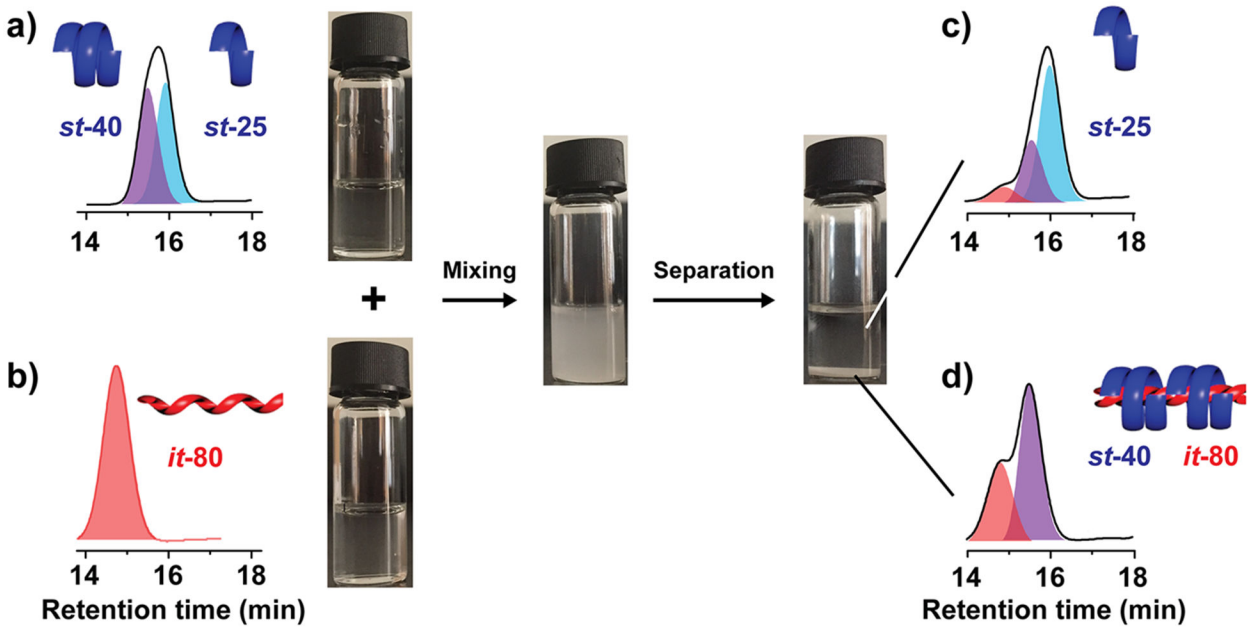

Figure 7.

Schematic illustrates the binding selectivity of OMMA toward high MW complementary species. Samples and GPC dRI traces of (a) 50:50 wt % mixture of *st*-25 and *st*-40, (b) *it*-80, (c) the supernatant, and (d) the precipitate collected after mixing the initial OMMA solutions (*it*-/*st*-molar ratio = 1:4).

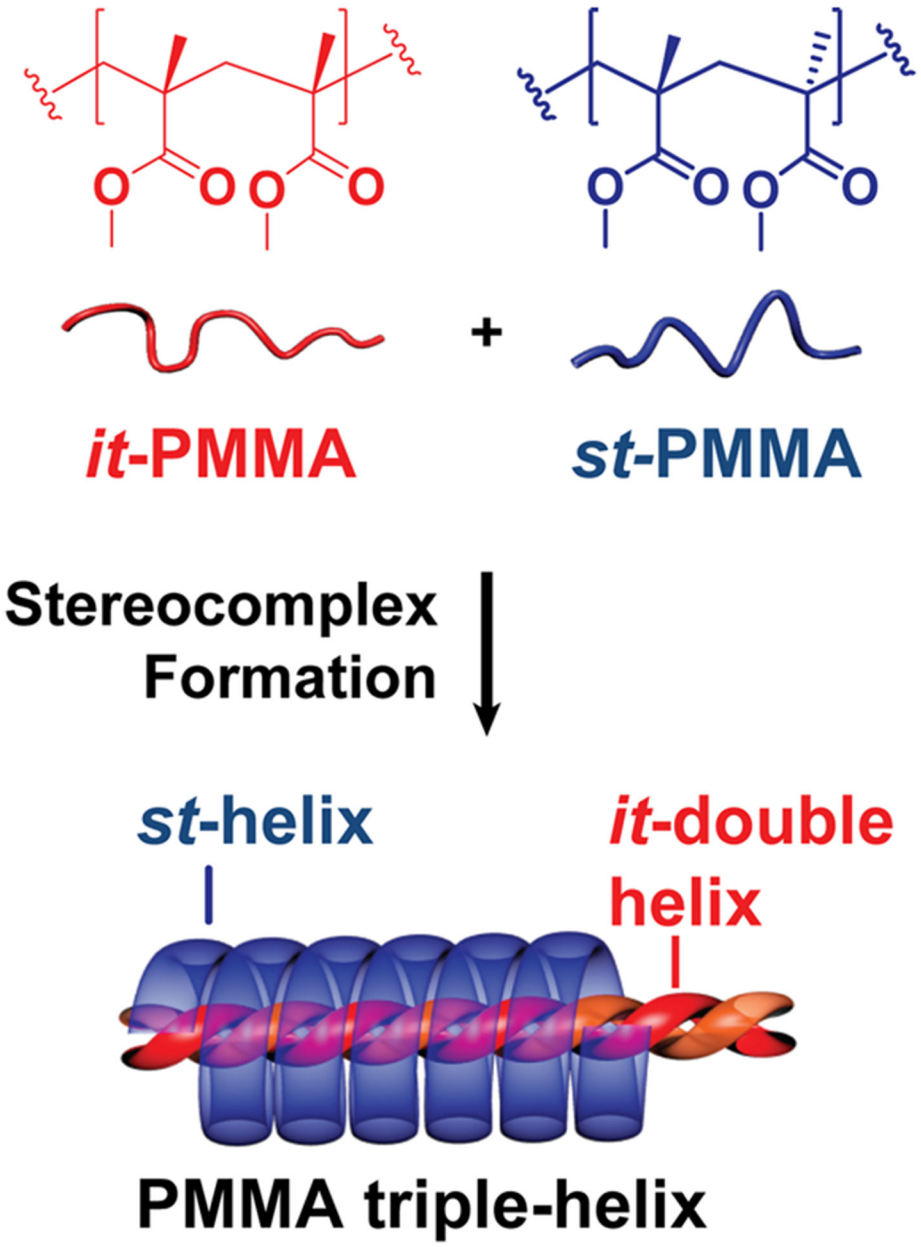

Scheme 1.
Illustration of PMMA Triple-Helix Stereocomplex Formation

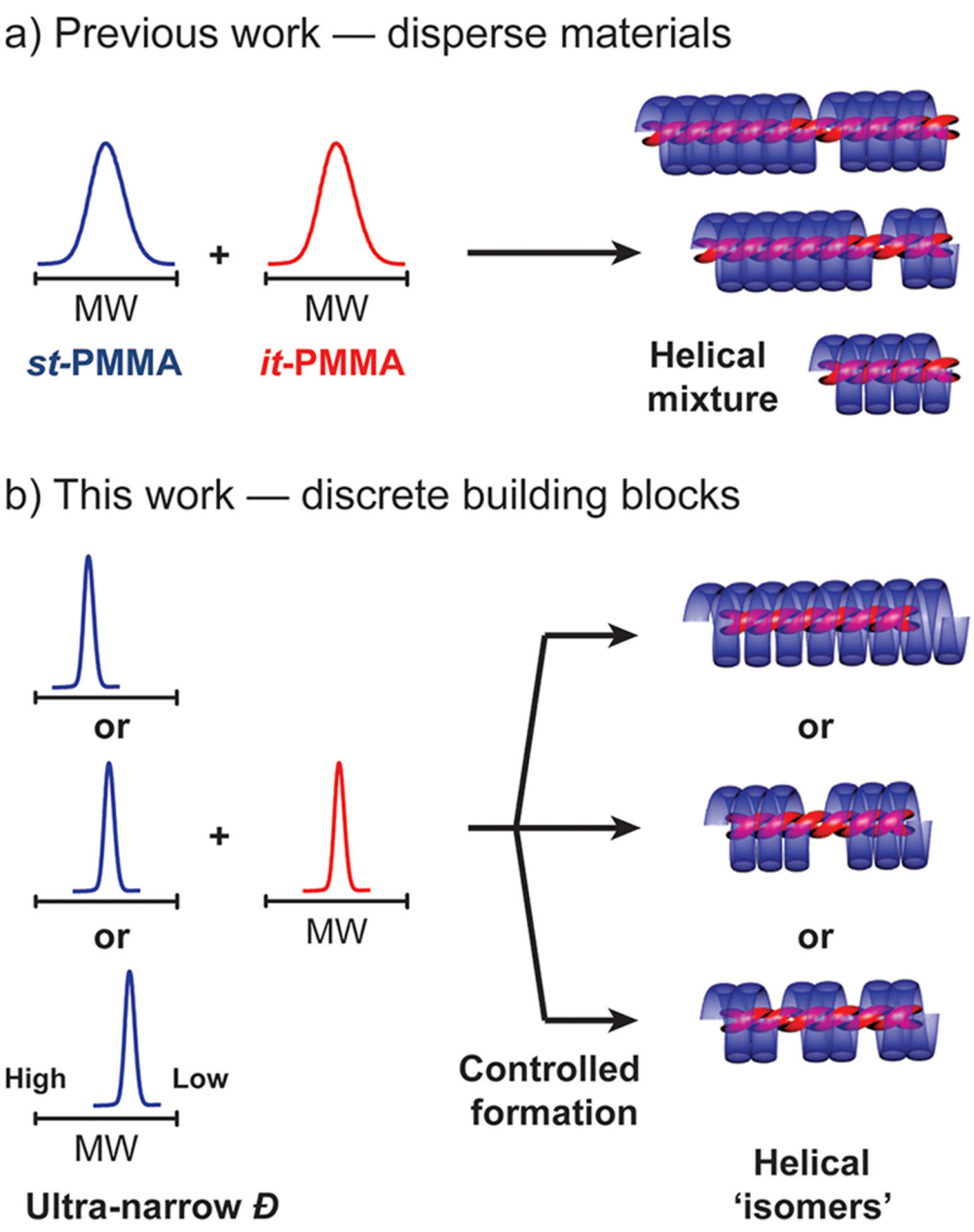

Scheme 2.

Illustration of (a) PMMA Stereocomplexes Prepared from Disperse Materials; (b) Designer PMMA Stereocomplexes Prepared from Discrete Building Blocks

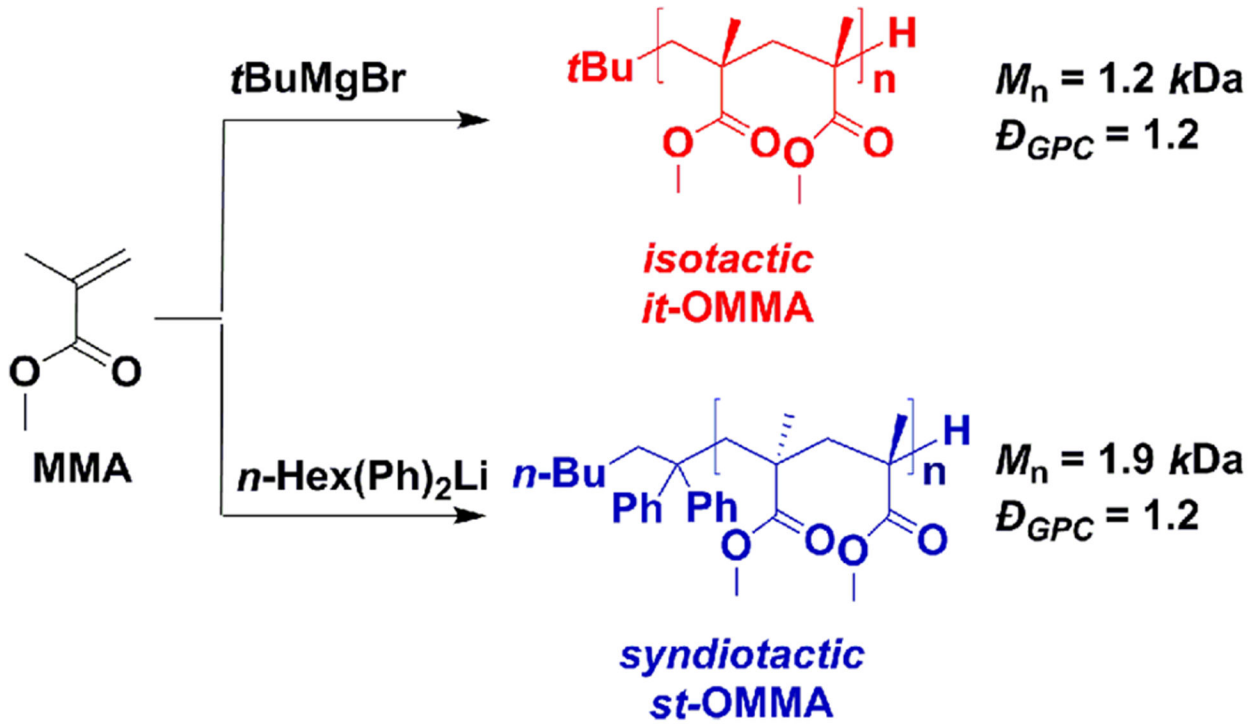

Scheme 3.
Synthesis of *Isotactic* (*it*-) and *Syndiotactic* (*st*-) Oligo(methyl methacrylate)s (OMMA)s

Table 1.

Characterization Summary of Stereoregular OMMA Samples

Sample	$M_{n,MALDI}$ [a]	$M_{n,NMR}$ [b]	$M_{n,GPC}$ [c]	$Đ_{MALDI}$ [d]	Tacticity [e]		
					mm	mr	rr
isotactic (it-)							
it-5	559	560	600	1.000	80	10	10
it-10	1100	1100	1200	1.001	80	10	10
it-15	1600	1500	1800	1.002	91	7	2
it-20	2100	2200	2500	1.003	90	8	2
it-30	3000	2800	3700	1.006	92	5	3
it-40	4000	3700	4900	1.003	88	7	5
it-60	6100	6000	7900	1.008	89	6	5
syndiotactic (st-)							
st-10	1240	1200	1300	1.000	1	24	75
st-15	1800	1900	1900	1.002	13	12	75
st-20	2300	2600	2700	1.005	10	13	77
st-30	3300	3400	3800	1.009	8	14	78
st-40	4300	4500	4700	1.009	7	14	79
st-60	6400	6000	7100	1.016	4	15	81

[a] Number-average molecular weight calculated based on MALDI-ToF MS analysis.

[b] Number-average molecular weight calculated based on NMR analysis.

[c] Number-average molecular weight calculated based on GPC analysis.

[d] Sample dispersity determined from MALDI-ToF MS analysis.

[e] Triad tacticity (mm, mr, and rr) calculated based on ^{1}H or ^{13}C NMR analysis (see SI).